

OMUDA: Omni-level Masking for Unsupervised Domain Adaptation in Semantic Segmentation

Yang Ou, *Member, IEEE*, Xiongwei Zhao[†], *Member, IEEE*, Xinye Yang, Yihan Wang, Yicheng Di, Rong Yuan, Xieyuanli Chen, *Member, IEEE*, Xu Zhu, *Senior Member, IEEE*

Abstract—Unsupervised domain adaptation (UDA) enables semantic segmentation models to generalize from a labeled source domain to an unlabeled target domain. However, existing UDA methods still struggle to bridge the domain gap due to cross-domain contextual ambiguity, inconsistent feature representations, and class-wise pseudo-label noise. To address these challenges, we propose Omni-level Masking for Unsupervised Domain Adaptation (OMUDA), a unified framework that introduces hierarchical masking strategies across distinct representation levels. Specifically, OMUDA comprises: 1) a Context-Aware Masking (CAM) strategy that adaptively distinguishes foreground from background to balance global context and local details; 2) a Feature Distillation Masking (FDM) strategy that enhances robust and consistent feature learning through knowledge transfer from pre-trained models; and 3) a Class Decoupling Masking (CDM) strategy that mitigates the impact of noisy pseudo-labels by explicitly modeling class-wise uncertainty. This hierarchical masking paradigm effectively reduces the domain shift at the contextual, representational, and categorical levels, providing a unified solution beyond existing approaches. Extensive experiments on multiple challenging cross-domain semantic segmentation benchmarks validate the effectiveness of OMUDA. Notably, on the SYNTHIA→Cityscapes and GTA5→Cityscapes tasks, OMUDA can be seamlessly integrated into existing UDA methods and consistently achieving state-of-the-art results with an average improvement of 7%.

Index Terms—Unsupervised Domain Adaptation, Semantic Segmentation, Omni Masks, Knowledge Transfer.

I. INTRODUCTION

SEMANTIC segmentation, a fundamental task in computer vision, aims to assign a semantic category to each pixel in an image. Recent advancements in deep learning-based methods have shown remarkable success in this field [1]–[6].

Yang Ou and Rong Yuan are with the School of Mechanical Engineering, Chengdu University, Chengdu 610106, China (e-mail: ouyang@my.swjtu.edu.cn, Yuanrong@cdu.edu.cn).

Xiongwei Zhao and Xu Zhu are with the School of Information Science and Technology, Harbin Institute of Technology, Shenzhen 518055, China (email: xwzhao@stu.hit.edu.cn, xuzhu@ieee.org)

Xinye Yang is with the School of Computer Science and Informatics, Cardiff University, Cardiff CF24 4AG, United Kingdom (email: yangxinye333@gmail.com)

Yihan Wang is with the School of Mechanical Engineering, Southwest Jiaotong University, Chengdu 610031, China (email: wyh123@my.swjtu.edu.cn)

Yicheng Di is with the School of Artificial Intelligence and Computer Science, Jiangnan University, Wuxi, China (email: diyicheng@stu.jiangnan.edu.cn)

Xieyuanli Chen is with the College of Intelligence Science and Technology, National University of Defense Technology, Changsha 410073, China (email: xieyuanli.chen@nudt.edu.cn).

[†] indicates Corresponding author.

However, such success heavily depends on large-scale annotated training data, whose collection is both labor-intensive and time-consuming [7]–[9]. To alleviate this annotation burden, researchers have explored leveraging synthetic data to train semantic segmentation models [10]–[12]. Although synthetic data offers a cost-effective alternative to manual annotation, models trained solely on synthetic images often generalize poorly to real-world domains due to the substantial domain gap between synthetic and real data distributions.

To address the above limitations, unsupervised domain adaptation (UDA) methods [13], [14] have been developed to transfer pixel-level knowledge from a labeled source domain to an unlabeled target domain. However, existing UDA methods [15]–[18] typically adopt a uniform strategy for all classes, ignoring the substantial differences between foreground and background categories. Background classes dominate the pixel distribution and largely determine the scene type, thereby providing rich contextual cues. In contrast, foreground classes have well-defined shapes and object boundaries but contribute less to global context. Despite their distinct characteristics, both background and foreground classes are crucial for comprehensive scene understanding. However, as illustrated in Fig. 1, empirical results of existing UDA methods show that they behave quite differently during training: (1) Compared with background classes, foreground categories (e.g., truck, train) exhibit much larger performance fluctuations across trials, as shown in Fig. 1(a), and form less stable contextual and spatial structures, whereas background classes maintain coherent layouts and strong contextual dependencies, as illustrated in Fig. 1(b). (2) foreground classes are more vulnerable to early performance degradation due to overfitting, given their limited and diverse samples, as demonstrated in Fig. 1(c); (3) large disparities in per-class accuracy lead to heterogeneous pseudo-label reliability across categories, as illustrated in Fig. 1(d). These issues limit the performance of existing UDA methods on semantic segmentation, and naturally motivate the design of diversified masking strategies that treat different semantic categories.

To address the aforementioned challenges, we propose Omni-level Masking for Unsupervised Domain Adaptation (OMUDA) for semantic segmentation, where Omni-level indicates that the proposed framework operates jointly at the contextual, representational, and categorical levels of adaptation. First, we introduce a Context-Aware Masking (CAM) strategy that combines class-aware sampling with distinct masking for foreground and background regions. CAM assigns different sampling weights to each class according to its

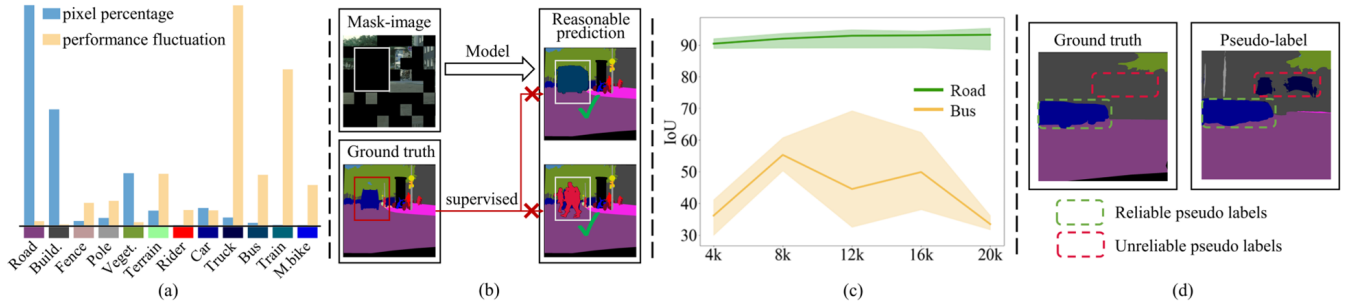


Fig. 1. Key inconsistency issues in existing UDA methods [19]–[21]. (a) Class performance fluctuation is inversely correlated with pixel frequency, with foreground classes showing higher instability. (b) Uniform masking disrupts critical background context and misguides supervision of foreground regions. (c) Background features remain stable during training, whereas foreground features easily drift and overfit. (d) Pseudo-label reliability varies across classes, with rare or complex categories exhibiting more errors.

pixel occupancy, and then applies coarse-grained masking to background regions to preserve global context and fine-grained masking to foreground regions to retain object-level details. Next, to reduce early overfitting and feature instability in foreground classes, we design the Feature Distillation Masking (FDM) strategy, which leverages generalized features from a pre-trained model to constrain foreground predictions during training. This encourages the model to learn more stable and consistent representations for domain-sensitive classes, particularly rare or small objects. Finally, to handle the varying reliability of pseudo-labels across categories, we propose the Class Decoupling Masking (CDM) strategy. CDM introduces a class-wise weighting mechanism that accounts for differences in confidence and accuracy, down-weighting unreliable pseudo-labels from difficult-to-adapt classes and thereby mitigating their negative impact during training. By integrating these three complementary strategies, OMUDA provides a robust and generalizable solution for UDA in semantic segmentation, with broad applicability to domain-shift scenarios in computer vision. Our contributions in this paper are summarized as follows:

- We propose Omni-level Masking for Unsupervised Domain Adaptation (OMUDA) for semantic segmentation, which introduces a hierarchical masking framework to enhance cross-domain knowledge transfer and alleviate performance degradation caused by domain shifts.
- We develop three complementary masking strategies acting at the contextual, representational, and categorical levels, respectively, effectively addressing foreground–background discrepancies, instability in foreground representations, and class-wise pseudo-label inconsistency within a unified framework.
- Extensive experiments on standard UDA benchmarks demonstrate that OMUDA can be seamlessly integrated into existing methods, consistently boosting their performance and achieving state-of-the-art results for semantic segmentation under domain shift.

The remainder of the paper is organized as follows. Section II reviews related work. Section III describes the proposed OMUDA framework and its three masking strategies. Section IV presents experimental results and ablation studies.

Finally, Section V concludes the paper.

II. RELATED WORK

A. Semantic Segmentation

Recent advances in deep learning have significantly enhanced the accuracy and efficiency of semantic segmentation models [22]–[24]. The authors of [25] and [26] proposed fully supervised methods that exploit global pixel-level relationships by extracting features across multiple images to regularize the segmentation embedding space. The authors of [27] introduced a unified attention fusion module, which leverages both spatial and channel attention to compute adaptive weights for feature fusion, enhancing representational capacity while maintaining lightweight efficiency. The authors of [28] proposed a contrastive learning-based semantic segmentation method that allows to capture local/global contexts and comprehend their relationships. However, the success of these methods often relies on large-scale annotated datasets, which are expensive and labor-intensive to obtain in real-world scenarios. To alleviate this issue, synthetic datasets [3], [10], [29] with dense annotations are commonly used as the labeled source domain. However, the domain gap between synthetic and real-world data, caused by differences in lighting, weather, sensor configurations, or geographic environments, still remains a major challenge.

B. Unsupervised Domain Adaptation (UDA)

Unsupervised domain adaptation (UDA) for semantic segmentation has been proposed to transfer knowledge from a labeled source domain to an unlabeled target domain, without requiring manual annotations. Existing UDA approaches for semantic segmentation can be broadly categorized into two main approaches: adversarial learning and self-learning [30]–[32]. Adversarial training aims to reduce the distribution gap between source and target domains by aligning feature representations [33], [34]. Following the success of generative adversarial networks (GANs), these approaches typically employ a domain discriminator to distinguish source from target features, while the segmentation network is trained to generate domain-invariant representations [35], [36]. More recently,

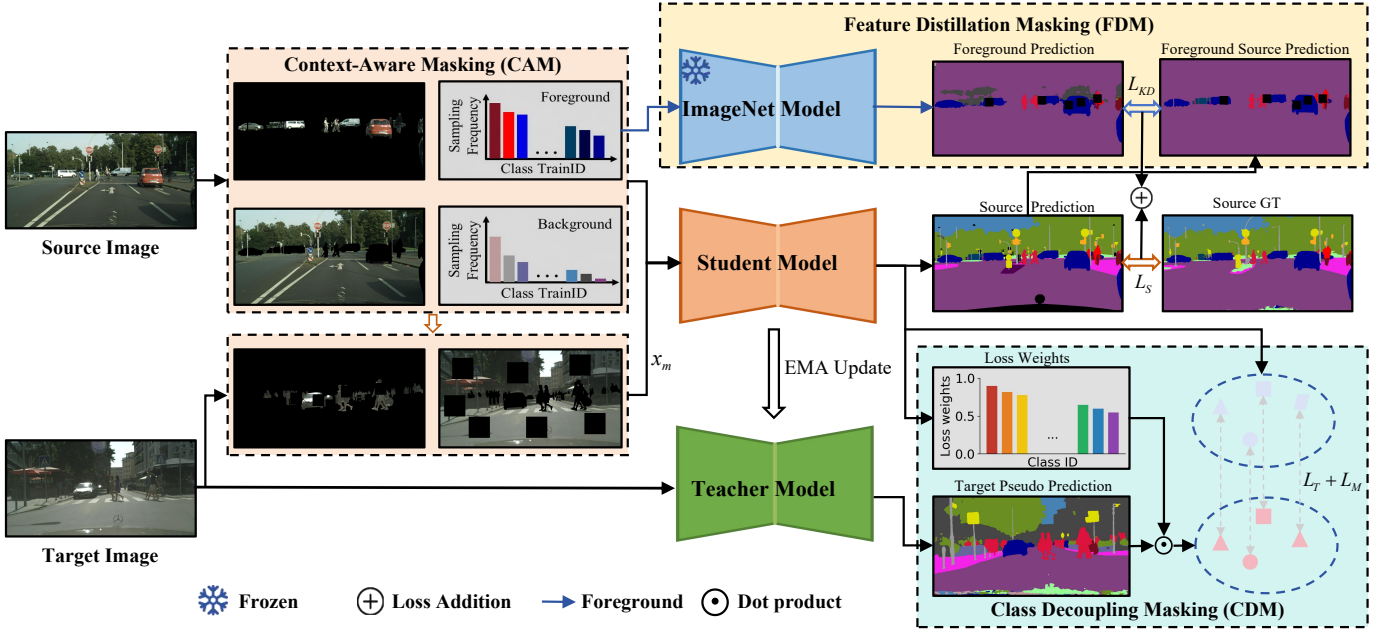


Fig. 2. Overview of the proposed OMUDA framework. The framework integrates three modules: CAM for class-aware sampling and masking, FDM for foreground feature distillation using a pretrained ImageNet model, and CDM for class-wise reliability weighting and pseudo-label refinement. A student–teacher architecture with EMA updates enhances stability and effectiveness in unsupervised domain adaptation for semantic segmentation.

class-conditional adversarial approaches focus on aligning features within the same category rather than enforcing strict global alignment, as effective adaptation can be achieved when features are well separated across classes [37], [38]. Despite their progress, adversarial training approaches [39] often suffer from instability, mode collapse, and sensitivity to discriminator design, leading to suboptimal segmentation performance. In contrast, self-training approaches [40]–[42] have recently become the dominant paradigm. They typically use a model trained on the labeled source domain to generate pseudo-labels for unlabeled target images, which are then exploited for iterative re-training. However, due to the substantial distribution discrepancy between source and target domains, the generated pseudo-labels inevitably contain noise, leading to error accumulation and potential performance degradation.

C. Enhancing Self-training Approaches in UDA

To mitigate the issue of pseudo-label drift in self-training, various regularization strategies have been proposed. A common line of work focuses on confidence-based filtering, where only high-confidence pseudo-labels are retained for retraining [43]–[45]. Beyond simple thresholding, prototype-based methods introduce sample-wise pseudo-label correction [46], [47], leveraging class prototypes to refine noisy predictions and improve label reliability. In parallel, other studies have incorporated additional learning constraints to stabilize training. Consistency regularization encourages the model to produce invariant predictions under diverse perturbations of the same input [48], [49], while contrastive learning enhances feature discriminability by explicitly separating positive and negative pairs [50], [51]. Moreover, cross-domain mixup [52], [53] has been proposed as a data augmentation technique to create

interpolated samples between the source and target domains, thereby smoothing the transition between domains. Uncertainty estimation [54]–[57] has also been utilized to assess the reliability of pseudo-labels and guide the adaptation process. However, a key limitation of existing approaches is that they typically treat all classes uniformly, overlooking the distinct adaptation behaviors of foreground and background categories. This one-size-fits-all paradigm is often suboptimal, as semantic classes exhibit varying degrees of domain shift and adaptation difficulty.

III. METHODOLOGY

In this section, we first present the problem statement of UDA semantic segmentation, followed by a detailed introduction of our proposed OMUDA framework. The Pipeline overview of our OMUDA framework is shown in Fig. 2. As illustrated in Fig. 2, OMUDA comprises three key masking strategies: Context-Aware Masking (CAM), Feature Distillation Masking (FDM), and Class Decoupling Masking (CDM). The details of each component are described below.

A. Problem Statement

Unsupervised domain adaptation (UDA) semantic segmentation contains two datasets: a labeled source dataset $\mathbb{D}_s = \{(x_s^n, y_s^n)\}_{n=1}^{N_s}$ and an unlabeled target dataset $\mathbb{D}_t = \{x_t^m\}_{m=1}^{N_t}$. Each image $x \in \mathbb{R}^{H \times W}$ has height H and width W , and the corresponding source annotation $y_s^n \in \{0, 1\}^{H \times W \times K}$ is a one-hot label map over K semantic classes. Although the sizes N_s and N_t may differ, both domains share the same label space of K classes. The goal of UDA semantic segmentation is to learn a domain-invariant segmentation

network φ that performs well on the target domain by jointly exploiting \mathbb{D}_s and \mathbb{D}_t .

In practice, a network φ trained only on \mathbb{D}_s often generalizes poorly to \mathbb{D}_t due to the domain gap. To mitigate this issue, self-training UDA methods generate pseudo labels \hat{y}_t for target images and optimize a combined cross-entropy (CE) loss on source and target data. For a source image x_s with label y_s and a target image x_t with pseudo label \hat{y}_t , the CE loss can be written as:

$$\mathcal{L}_{ce} = - \sum_{i=1}^{H \times W} \sum_{k=1}^K y_s^{(i,k)} \log \varphi(x_s)^{(i,k)} + \hat{y}_t^{(i,k)} \log \varphi(x_t)^{(i,k)} \quad (1)$$

where $\hat{y}_t^{(i,k)} = \arg \max_k \phi(x_t)^{(i,k)}$ is the pseudo label predicted by the teacher network ϕ . The teacher network ϕ is not updated by backpropagation, but instead by the exponentially moving average (EMA) of the student segmentation network φ after each step j :

$$\phi_{j+1} = \alpha \phi_j + (1 - \alpha) \varphi_j \quad (2)$$

where $\alpha \in [0, 1)$ is the EMA decay factor.

B. Context-Aware Masking (CAM)

Substantial variations in performance fluctuation are observed across different classes. As illustrated in Fig.1(a), the fluctuation magnitude is inversely correlated with the percentage of pixels belonging to each class. Foreground classes, which typically occupy smaller regions and contain fewer pixels, exhibit significantly higher performance volatility than background classes. In this work, we follow the common distinction in semantic segmentation between object and background categories: foreground classes refer to object categories with clear instance boundaries (e.g., person, rider, car), whereas background classes correspond to large, layout-defining regions (e.g., road, building, sky). This observation suggests that class imbalance is a major contributing factor to unstable learning. Motivated by this observation, we assign class-specific sampling weights based on pixel occupancy. We first compute the pixel frequency f_k of class k as the proportion of pixels labeled as class k over the source domain:

$$f_k = \frac{\sum_{n=1}^{N_s} \sum_{i=1}^{H \times W} \mathbb{I}[y_s^{(i,n)} = k]}{N_s \times H \times W} \quad (3)$$

To better accommodate the distinct characteristics of foreground and background classes, we decouple them and compute their sampling probabilities separately:

$$P_b(k) = \frac{e^{(1-f_k)/T_b}}{\sum_{k'=1}^{K_b} e^{(1-f_{k'})/T_b}} \quad (4)$$

$$P_f(k) = \frac{e^{(1-f_k)/T_f}}{\sum_{k'=1}^{K_f} e^{(1-f_{k'})/T_f}} \quad (5)$$

where T_b and T_f control the smoothness of the sampling distribution for background and foreground classes, respectively, while K_b and K_f denote the number of background and foreground classes. The final sampling distribution is given by $P = \{P_b, P_f\}$. In all experiments, we set $T_b = 1.0$

and $T_f = 0.7$ to provide a moderate re-balancing effect for background classes while more strongly emphasizing rare foreground categories.

On the other hand, foreground classes typically lack strong contextual dependencies among themselves. In UDA semantic segmentation, this further complicates representation learning because standard masking strategies (e.g., random or grid-based masking) treat all regions uniformly and overlook the distinct roles of foreground and background. As shown in Fig. 1(b), such indiscriminate masking can disrupt essential background structures (e.g., road or sky), which provide key contextual cues, leading to semantic inconsistencies such as misclassifying a ‘‘car’’ as a ‘‘person’’. To address this issue, we obtain pseudo labels \hat{y}_t from the teacher network ϕ and partition each image into foreground and background regions based on the predefined class sets K_f and K_b . We then apply a coarse-grained mask \mathcal{M}_b to background regions and a fine-grained mask \mathcal{M}_f to foreground regions:

$$\begin{aligned} x_{t_b} &= \mathcal{M}_b \odot x_t, \\ x_{t_f} &= \mathcal{M}_f \odot x_t, \end{aligned} \quad (6)$$

where \odot denotes element-wise multiplication. The final masked image x_m is obtained by combining x_{t_b} and x_{t_f} based on the pseudo labels:

$$x_m = x_{t_b} \odot \mathbb{I}[\hat{y}_t^{(i,k)} \in K_b] + x_{t_f} \odot \mathbb{I}[\hat{y}_t^{(i,k)} \in K_f] \quad (7)$$

The CAM strategy first performs class-aware sampling and then applies distinct masking patterns to background and foreground regions, enabling the model to better capture their differing characteristics while reducing its over-reliance on background context during training. Unlike DACS [52], which adopts a uniform class-mixing scheme for all categories, CAM explicitly decouples foreground and background classes and tailors the masking process to their semantic roles in the scene.

C. Feature Distillation Masking (FDM)

During the training process, the model distinguishes classes by learning discriminative features from the input data. However, as illustrated in Fig. 1(c), background features tend to be more stable, while foreground features exhibit greater variability and are more susceptible to overfitting. This instability comes mainly from two factors. First, foreground classes contain far fewer instances than background classes, limiting the data available for learning robust representations. Second, foreground categories often display more complex and diverse visual appearances, making it difficult for the model to learn generalizable features. Such unstable foreground representations ultimately hinder semantic segmentation performance.

To mitigate this issue, we leverage a pretrained feature extractor E_{pre} , trained on a large-scale dataset (e.g., ImageNet), to provide stable foreground feature priors. For each input, we obtain feature maps from both E_{pre} and the student model φ 's neck module E_{neck} , and introduce a feature distillation loss on foreground regions rather than relying solely on noisy pseudo-label supervision. Specifically, we distill both the feature distance and the angular relationship between foreground samples, which encourages E_{neck} to preserve the similarity

structure and geometric configuration of foreground embeddings. This regularization stabilizes foreground representations and effectively alleviates early overfitting and feature collapse. First, we compute the feature distance between different samples as:

$$d_{pre}^{(i,j)} = \frac{\|(f_{pre}^i - f_{pre}^j) M\|_2}{\sum_{(x_i, x_j) \in \mathbb{D}_s} \|(f_{pre}^i - f_{pre}^j) M\|_2} \quad (8)$$

$$\text{with } f_{pre}^i = E_{pre}(x_s^i), M = \mathbb{I}[y_s^{(i,k)} \in K_f]$$

where M is a mask that indicates the foreground classes in the image. Similarly, we compute $d_{neck}^{(i,j)}$ and the distance distillation loss function is defined as follows:

$$\mathcal{L}_D = \sum_{(x_i, x_j) \in \mathbb{D}_s} L_1(d_{pre}^{(i,j)} - d_{neck}^{(i,j)}) \quad (9)$$

$$\text{with } L_1(x) = \begin{cases} 0.5x^2 & \text{if } |x| < 1 \\ |x| - 0.5 & \text{otherwise} \end{cases}$$

The feature angle between different samples is calculated as follows:

$$a_{pre}^{i,j,k} = \left\langle \frac{(f_{pre}^i - f_{pre}^j) M}{\|(f_{pre}^i - f_{pre}^j) M\|_2}, \frac{(f_{pre}^i - f_{pre}^k) M}{\|(f_{pre}^i - f_{pre}^k) M\|_2} \right\rangle \quad (10)$$

where $\langle \cdot \rangle$ is the cosine similarity, and the angular distillation loss function is:

$$\mathcal{L}_A = \sum_{(x_i, x_j, x_k) \in \mathbb{D}_s} L_1(a_{pre}^{i,j,k} - a_{neck}^{i,j,k}) \quad (11)$$

The overall KD loss function is

$$\mathcal{L}_{KD} = \mathcal{L}_D + \mathcal{L}_A \quad (12)$$

Ultimately, \mathcal{L}_{KD} is added to the final loss function via a weighting factor λ_{KD} . The FDM strategy integrates the mask-based KD loss \mathcal{L}_{KD} into the training process, enhancing the student model's ability to generate accurate masks and improving its segmentation and localization performance. This leads to more reliable and precise semantic segmentation results.

D. Class Decoupling Masking (CDM)

Fig. 1(d) further shows that pseudo-label reliability varies substantially across classes. This variability stems from factors such as domain shift, distribution mismatch, and model uncertainty. Some categories exhibit higher prediction uncertainty due to appearance variations, occlusion, or inherent semantic ambiguity, which results in more labeling errors. Consequently, pseudo-labels for these classes tend to be less reliable than those for more stable categories. To address this issue, we introduce a weighting strategy that assigns higher weights to the pseudo-label errors of difficult-to-adapt classes. This mitigates their adverse influence during training, as such classes are more susceptible to domain shift. We begin by normalizing the class-wise loss. The normalized loss \mathcal{L}_{norm} is obtained by summing over the spatial dimensions ($H \times W$) and the classes (K), while using the indicator function $\mathbb{I}[\hat{y}^{(i)} = k]$

to ensure that only the loss corresponding to the predicted class is counted. The formulation is given by:

$$\mathcal{L}_{norm} = \sum_{i=1}^{H \times W} \sum_{k=1}^K \frac{1}{\mathbb{I}[\hat{y}^{(i)} = k]} \hat{y}^{(i,k)} \log \varphi(x)^{(i,k)} \quad (13)$$

Next, we take into account the varying difficulty of migration across classes. We calculate a weighting factor β_k for each class k , which quantifies the uncertainty of each training sample. The weighting factor is computed by summing over the spatial dimensions ($H \times W$) and the samples (N_t), and using the indicator function to determine if the predicted label $p_k^{(i,n)}$ matches the pseudo-label $\hat{y}_k^{(i,n)}$. The equation for β_k is as follows:

$$\beta_k = \sum_{i=1}^{H \times W} \sum_{n=1}^{N_t} \left(1 - \frac{\mathbb{I}[p_k^{(i,n)} = \hat{y}_{k=1}^{(i,n)}]}{\mathbb{I}[\hat{y}_k^{(i,n)} = c]} \right) \quad (14)$$

Finally, we incorporate the class weighting into the loss function. The normalized loss \mathcal{L}_{norm} is multiplied by the weighting factor β_k , and the indicator function $\mathbb{I}[\hat{y}^{(i,k)} = j]$ is used to ensure that only the loss for the correct class is considered. The equation for the class weighting loss function is as follows:

$$\mathcal{L}_{w_norm} = \sum_{i=1}^{H \times W} \sum_{k=1}^K \frac{\beta_k}{\mathbb{I}[\hat{y}^{(i)} = k]} \hat{y}^{(i,k)} \log \varphi(x)^{(i,k)} \quad (15)$$

E. Loss Function

In our framework, the student network φ is trained with three types of supervision: fully supervised losses on the labeled source domain, feature distillation on source foreground regions, and pseudo-label based losses on the unlabeled target domain. On the source domain, we use the standard cross-entropy loss with ground-truth annotations, denoted as \mathcal{L}_S , and the foreground feature distillation loss \mathcal{L}_{KD} between the student neck E_{neck} and the pretrained feature extractor E_{pre} . On the target domain, we employ the class-weighted normalized loss \mathcal{L}_{w_norm} , using teacher-generated pseudo-labels as supervision, to obtain the loss on original target images \mathcal{L}_T and on their CAM-generated masked loss \mathcal{L}_M . Within the CDM module, \mathcal{L}_{w_norm} reweights classes according to their pseudo-label reliability, so that noisy and hard-to-adapt categories do not dominate the optimization. The overall training objective is:

$$\mathcal{L}_{Total} = \mathcal{L}_S + \lambda_{KD} \mathcal{L}_{KD} + \mathcal{L}_T + \mathcal{L}_M, \quad (16)$$

where λ_{KD} is the a weighting factor of KD loss, and its effect is further analyzed in the ablation studies in Section IV.

IV. EXPERIMENTAL RESULTS

A. Datasets and Implementation Details

We conduct our experimental evaluation on two widely adopted UDA benchmarks. The first uses synthetic source images from the GTA5 dataset [58], containing 24,966 images (1914×1052). The second employs SYNTHIA [59] as the source domain, which provides 9,400 images (1280×760). In both benchmarks, the target domain is Cityscapes [60],

Table I: Quantitative comparison with previous UDA methods on GTA5→Cityscapes benchmark. The best results are highlighted in bold while the second best results are shown by underline.

	Road	S.walk	Build.	Wall	Fence	Pole	Tt.Light	Sign	Veget.	Terrain	Sky	Person	Rider	Car	Truck	Bus	Train	M.bike	Bike	mIoU
GTA5 → Cityscapes																				
FADA [66]	92.5	47.5	85.1	37.6	32.8	33.4	33.8	18.4	85.3	37.7	83.5	63.2	39.7	87.5	32.9	47.8	1.6	34.9	39.5	49.2
Uncertainty [57]	90.4	31.2	85.1	36.9	25.6	37.5	48.8	48.5	85.3	34.8	81.1	64.4	36.8	86.3	34.9	52.2	1.7	29.0	44.6	50.3
FDA [67]	92.5	53.3	82.4	26.5	27.6	36.4	40.6	38.9	82.3	39.8	78.0	62.6	34.4	84.9	34.1	53.1	16.9	27.7	46.4	50.5
DACS [52]	89.9	39.7	87.9	30.7	39.5	38.5	46.4	52.8	88.0	44.0	88.8	67.2	35.8	84.5	45.7	50.2	0.0	27.3	34.0	52.1
CorDA [68]	94.7	63.1	87.6	30.7	40.6	40.2	47.8	51.6	87.6	47.0	89.7	66.7	35.9	90.2	48.9	57.5	0.0	39.8	56.0	56.6
ProDA [46]	87.8	56.0	79.7	46.3	44.8	45.6	53.5	53.5	88.6	45.2	82.1	70.7	39.2	88.8	45.5	59.4	1.0	48.9	56.4	57.5
CONFETI [69]	96.5	75.6	88.9	45.1	45.9	50.1	61.2	68.2	89.4	45.7	86.3	76.3	49.9	92.2	55.1	62.8	16.7	33.8	63.1	63.3
IDM [70]	97.2	77.1	89.8	51.7	<u>51.7</u>	<u>54.5</u>	59.7	64.7	89.2	45.3	90.5	<u>74.2</u>	46.6	92.3	76.9	<u>81.2</u>	57.3	62.4	69.5	
DAFormer [61]	95.7	70.2	89.4	53.5	48.1	49.6	55.8	59.4	89.9	47.9	<u>92.5</u>	72.2	44.7	92.3	74.5	78.2	65.1	55.9	61.8	68.3
DAFormer+FST [19]	95.3	67.7	89.3	<u>55.5</u>	47.1	50.1	57.2	58.6	89.9	51.0	92.9	72.7	46.3	92.5	78.0	81.6	74.4	57.7	62.6	69.3
DAFormer+CAMix [20]	96.0	73.1	89.5	53.9	50.8	51.7	58.7	64.9	90.0	<u>51.2</u>	92.2	71.8	44.0	92.8	78.7	82.3	70.9	54.1	<u>64.3</u>	70.0
DAFormer+MICDrop [21]	96.0	71.8	<u>90.3</u>	53.3	46.4	54.8	57.8	<u>66.7</u>	<u>90.0</u>	49.2	92.2	73.6	46.3	<u>92.8</u>	<u>78.1</u>	80.6	70.7	<u>57.5</u>	<u>63.2</u>	<u>70.1</u>
DAFormer+OMUDA	<u>96.9</u>	<u>76.6</u>	90.8	59.8	52.3	54.1	<u>59.7</u>	64.9	90.9	51.7	92.3	73.1	<u>49.3</u>	93.5	77.7	82.9	81.6	54.6	64.9	72.0

Table II: Quantitative comparison with previous UDA methods on SYNTHIA→Cityscapes benchmark. The best results are highlighted in bold while the second best results are shown by underline.

	Road	S.walk	Build.	Wall	Fence	Pole	Tt.Light	Sign	Veget.	Terrain	Sky	Person	Rider	Car	Truck	Bus	Train	M.bike	Bike	mIoU
SYNTHIA → Cityscapes																				
FADA [66]	84.5	40.1	83.1	4.8	0.0	34.3	20.1	27.2	84.8	–	84.0	53.5	22.6	85.4	–	43.7	–	26.8	27.8	45.2
Uncertainty [57]	87.6	41.9	83.1	14.7	1.7	36.2	31.3	19.9	81.6	–	80.6	63.0	21.8	86.2	–	40.7	–	23.6	53.1	47.9
CCM [71]	79.6	36.4	80.6	13.3	0.3	25.5	22.4	14.9	81.8	–	77.4	56.8	25.9	80.7	–	45.3	–	29.9	52.0	45.2
DACS [52]	80.6	25.1	81.9	21.5	2.9	37.2	22.7	24.0	83.7	–	90.8	67.6	38.3	82.9	–	38.9	–	28.5	47.6	48.3
CorDA [68]	93.3	61.6	85.3	19.6	5.1	37.8	36.6	42.8	84.9	–	90.4	69.7	41.8	85.6	–	38.4	–	32.6	53.9	55.0
ProDA [46]	87.8	45.7	84.6	37.1	0.6	44.0	54.6	37.0	88.1	–	84.4	<u>74.2</u>	24.3	88.2	–	51.1	–	40.5	45.6	55.5
CONFETI [69]	83.8	44.6	86.9	15.4	3.7	44.3	56.9	55.5	84.9	–	86.2	<u>73.8</u>	46.8	90.1	–	57.1	–	46.0	63.2	58.7
IDM [70]	87.6	47.6	88.1	33.4	6.3	52.8	<u>57.8</u>	56.5	83.0	–	77.5	66.2	<u>52.1</u>	<u>89.3</u>	–	55.6	–	<u>57.1</u>	64.2	60.9
DAFormer [61]	84.5	40.7	88.4	41.5	6.5	50.0	55.0	54.6	86.0	–	89.8	73.2	48.2	87.2	–	53.2	–	53.9	61.7	60.9
DAFormer+FST [19]	88.3	46.1	88.0	41.7	7.3	50.1	53.6	52.5	<u>87.4</u>	–	<u>91.5</u>	73.9	48.1	85.3	–	58.6	–	55.9	<u>63.4</u>	61.9
DAFormer+MICDrop [21]	81.0	37.1	<u>89.4</u>	<u>45.7</u>	9.5	51.8	57.3	<u>58.0</u>	86.7	–	85.0	73.6	50.4	88.2	–	64.7	–	56.8	62.8	<u>62.4</u>
DAFormer+OMUDA	<u>88.5</u>	<u>51.9</u>	89.6	49.8	<u>7.9</u>	<u>52.4</u>	59.2	58.6	86.2	–	92.8	76.2	54.0	88.9	–	<u>64.2</u>	–	57.9	61.8	65.0

consisting of 500 validation images (2048×1024). Following prior work [19], [52], [61], we report mIoU over the 19 classes shared by GTA5→Cityscapes and the 16 classes shared by SYNTHIA→Cityscapes. We use DAFormer [61] as our baseline model, as it achieves a strong performance at high training and inference speed. For pretrained feature extraction, we adopt MiT-B5 [62] pretrained on ImageNet [63].

We adopt AdamW [64] with betas (0.9, 0.999) as the optimizer, a learning rate of 6×10^{-5} for the encoder and 6×10^{-4} for the decoder, a linear learning rate warmup [65] of 1.5k iterations, a weight decay of 0.01. Following DAFormer [61], we resize target images to 1024×512 and source images to 1280×720 , with a random crop size of 512×512 . The model is trained for 40k iterations with the batch size of 3. All experiments are conducted on one NVIDIA GeForce RTX 3090 and implemented with the PyTorch framework.

B. Comparison with the State-of-the-art Approaches

In this section, we compare the performance of the proposed OMUDA with those of the state-of-the-art UDA methods on GTA5→Cityscapes and SYNTHIA→Cityscapes, respectively. Specifically, we use FADA (ECCV’2020) [66],

Table III: Quantitative comparison with previous UDA methods on GTA5→Cityscapes and SYNTHIA→Cityscapes benchmark. The best mIoU results are highlighted in bold while the second best results are shown by underline.

	GTA5 → Cityscapes	SYNTHIA → Cityscapes
VLTSeg [72]	62.6	56.8
TQDM [73]	68.9	58.0
DPMFormer [74]	<u>70.1</u>	<u>58.9</u>
DAFormer+OMUDA	72.0	65.0

Uncertainty (IJCV’2021) [57], FDA (CVPR’2020) [67], DACS (IWACACV’2021) [52], CorDA (CVPR’2021) [68], ProDA (CVPR’2021) [46], DAFormer(2022’CVPR) [61], DAFormer+FST (NIPS’2022) [19], DAFormer+CAMix (TCSVT’2022) [20], CONFETI (CVPR’2023) [69], IDM (CVPR’2023) [70], VLTSeg (arXiv’2023) [72], DAFormer+MICDrop (ECCV’2024) [21], TQDM (ECCV’2024) [73], DPMFormer (CVPR’2025) [74]. Quantitative comparisons are shown in Table I to Table III.

1) *GTA5→Cityscapes*: First, we present our results on GTA→Cityscapes in Table I and highlight the best results in bold. Generally, our OMUDA achieves 72.0

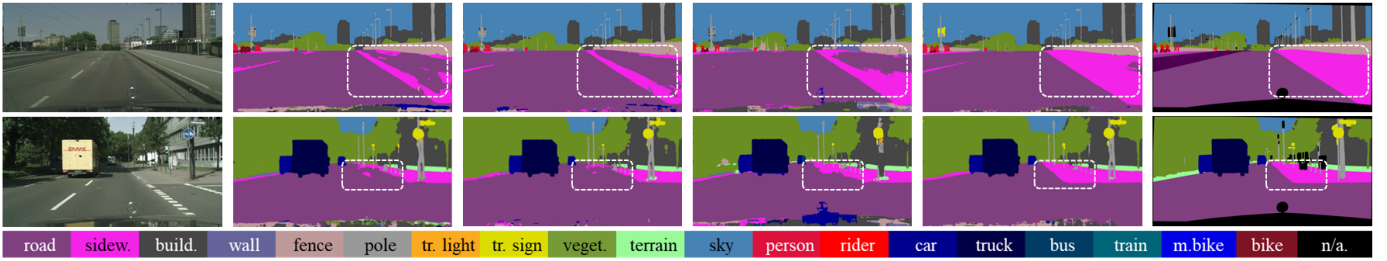


Fig. 3. Qualitative results on GTA5→Cityscapes. From left to right: Target image, the visual results predicted by DAFormer, DAFormer+FST, DPMFormer, DAFormer+OMUDA (ours), and Ground Truth. We deploy the white rectangles highlight the visual improvements. OMUDA better segments difficult classes, including sidewalk, terrain, traffic sign, and bus.

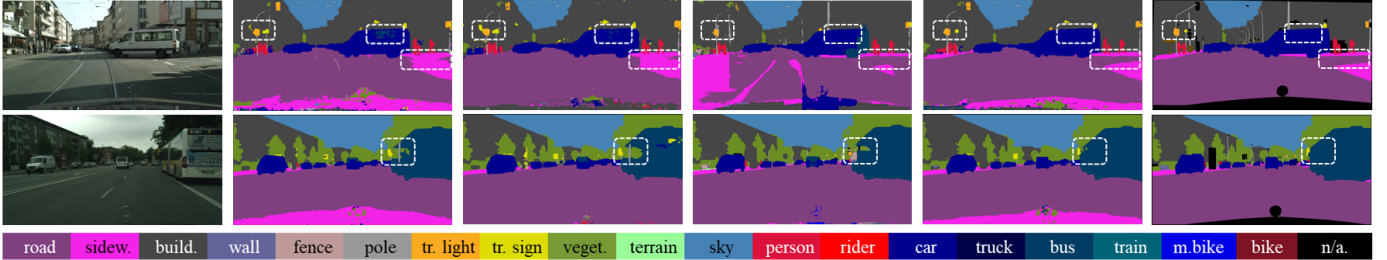


Fig. 4. Qualitative results on SYNTHIA→Cityscapes. From left to right: Target Image, the visual results predicted by DAFormer, DAFormer+FST, DPMFormer, DAFormer+OMUDA (Ours), and Ground Truth. We deploy the white rectangles highlight the visual improvements. OMUDA better segments difficult classes such as sidewalk, terrain, traffic sign, and bus.

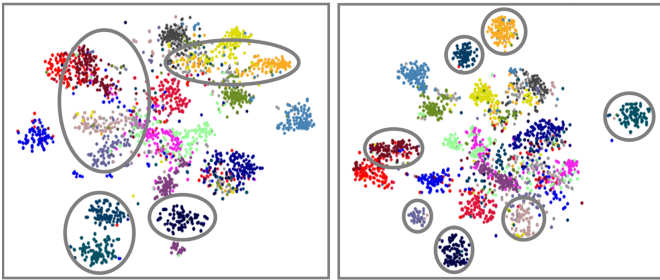


Fig. 5. T-SNE visualization of learned feature embeddings for DAFormer (left) and OMUDA (right) on Cityscapes dataset.

mIoU, yielding a significant improvement over the previous strongest transformer-based models, including DAFormer [61], DAFormer+FST [19], DAFormer+CAMix [20] and DAFormer+MICDrop [21]. Among all the 19 classes, we achieve the best scores on 9 classes and the second best scores on 4 classes including several hard objectives such as wall, fence, terrain, and train, which cannot be well handled in previous works. Particularly, we increase the IoU of the train by +7.2 from 74.4 to 81.6 mIoU. The IoU performance of OMUDA verifies our motivation that class decoupling indeed helps category recognition, especially for challenging small or rare objects.

2) *SYNTHIA*→*Cityscapes*: Table II displays the adaptation results on *SYNTHIA* → *Cityscapes*, demonstrating remarkable advancements achieved by OMUDA. The proposed OMUDA increases +4.1, +3.1, +2.6 mIoU compared with DAFormer [61], DAFormer+FST [19] and DAFormer+MICDrop [21], respectively. Among all the 16 classes, we achieve the best scores on 8 classes and the second best scores on 5 classes,

most of those are hard classes that previous approaches struggled to effectively address, e.g., wall, traffic light, person and rider. We have also report the comparison results of our ODMA method with VLTseg [72], TQDM [73], and DPMFormer [74] in Table III.

3) *Qualitative results*: Additionally, we provide qualitative results of our approach in comparison with DAFormer [61], DAFormer+FST [19] and DPMFormer [74], as depicted in Figs. 3 and 4. In these two Figs, we visualize the segmentation results and the comparison with previous strong methods DAFormer [61], DAFormer+FST [19] and DPMFormer [74], and the ground truth on GTA5→Cityscapes and SYNTHIA→Cityscapes benchmarka. The results highlighted by white dash boxes show that OMUDA corrects typical classes that cannot be well handled DAFormer, DAFormer+FST and DPMFormer, e.g. sidewalk, fence, and bus. Especially in the second row of Fig. 4, we can see that OMUDA is more complete and smoother in terms of object interiors and edge details. This outcome is attributed to class decoupling, wherein each class is trained based on its distinctive attributes. This strategy effectively alleviates class confusion and yields smoother edge predictions.

To better develop intuition, we draw T-SNE visualizations [75] of the learned feature representations for DAFormer and OMUDA in Fig. 5. From the T-SNE analysis, we can observe that although DAFormer can produce separated features, they are mainly focused on simple classes (e.g., sky) and the same class may produce multiple clusters of features (e.g., traffic light), while the interval between similar classes is not obvious (e.g., fence and wall), making it difficult to make dense predictions. With the implementation of class decoupling, features among different classes can achieve better

Table IV: Comparison of the class-wise IoU of each proposed component for GTA→Cityscapes.

	Road	S.walk	Build.	Wall	Fence	Pole	Tr.Light	Sign	Veget.	Terrain	Sky	Person	Rider	Car	Truck	Bus	Train	M.bike	Bike	mIoU
Baseline	95.7	70.2	89.4	53.5	48.1	49.6	55.8	59.4	89.9	47.9	92.5	72.2	44.7	92.3	74.5	78.2	65.1	55.9	61.8	68.3
+CAM	96.6	74.7	89.3	54.1	45.5	47.8	56.9	58.4	89.9	50.9	90.8	71.9	43.7	92.4	78.7	78.8	69.7	57.7	63.7	69.3
+FDM	96.0	71.9	89.7	55.4	49.1	49.8	56.0	62.2	89.9	49.8	90.3	72.8	42.6	92.5	78.8	79.1	71.6	57.7	63.4	69.1
+CDM	97.0	76.3	90.3	56.7	53.4	53.5	58.5	60.0	90.7	51.0	92.1	73.1	48.5	93.2	76.7	82.4	79.3	54.7	64.6	71.2
All	96.9	76.6	90.8	59.8	52.3	54.1	59.6	64.9	90.9	51.7	92.3	73.1	49.3	93.5	77.7	82.9	81.6	54.6	64.9	72.0

Table V: The effect of loss weight on GTA5→Cityscapes.

Strategy	Uniform	Fix radio	RCS	Ours
mIoU	69.8	71.5	71.6	72.0

intra-class compactness and inter-class separability, especially for classes that are usually particularly difficult to adapt, such as traffic light, fence, wall, truck, bus, and train. In contrast, the embedded representations of our OMUDA showcase the most distinct clusters when compared to those of DAFormer. This observation underscores the discriminative potential underpinning the class decoupling approach.

C. Ablation Study

In this section, a series of ablation studies are conducted to substantiate the individual contributions of each component to the ultimate performance. All experiments are performed on the GTA5→Cityscapes benchmark.

1) *Effect of Components*: We conduct a comprehensive series of experiments to assess the efficacy of the developed OMUDA framework and report the performance in Table IV. We take DAFormer [61] as our baseline. Based on the results, we note that each component significantly contributes to the overall performance of our framework. Notably, the inclusion of the CDM component yields the most substantial gain of +2.9 mIoU. Specifically, it can be seen from Table IV that adding the CAM sharply improves performance for difficult-to-adapt classes, such as sidewalk, terrain, truck, and train. And with the addition of the FDM, the performance improvement mainly comes from rare classes, especially in fence, pole, traffic signal, and train.

2) *Ablation Study on CAM*: We compare several data sampling strategies, including uniform sampling, a fixed sampling ratio, RCS (as adopted in DAFormer [61]), and our proposed CAM strategy. Table V summarizes the results. Across all evaluations, our approach consistently delivers superior performance, demonstrating its effectiveness over conventional sampling methods. Furthermore, we evaluate the effectiveness of our masking strategy by comparing it with random masking [76] and grid masking [77]. As shown in Table VI, CAM consistently outperforms both baselines, achieving gains of +0.6 mIoU over random masking and +0.8 mIoU over grid masking. Notably, different CAM configurations also impact performance: a finer-grained setting (16/32) yields the best result, reaching 72.0 mIoU. These findings demonstrate that

Table VI: The influence of different masking strategy on GTA5→Cityscapes.

Mask strategy	Fore-mask size	Back-mask size	mIoU
Random	–	–	70.6
Grid	–	–	70.4
CAM	32	64	70.9
CAM	16	32	72.0

Table VII: The effect of KD Loss Weight on GTA5→Cityscapes.

λ_{KD}	0.1	0.05	0.01	0.005
mIoU	69.4	70.2	72.0	70.1

context-aware masking not only surpasses conventional masking strategies but also benefits from carefully chosen mask granularity.

3) *Effect of the KD Loss Weight in the FDM*: Table VII reports the results obtained with different KD loss weights ($\lambda_{KD} \in 0.1, 0.05, 0.01, 0.005$). These results highlight the critical role of the KD loss in stabilizing feature learning within the FDM module. When the weight is too large, the student model focuses excessively on matching the pretrained features, which limits its ability to learn target-domain representations and leads to reduced adaptation performance. In contrast, if the weight is too small, the distillation signal becomes insufficient to regularize the model, making it prone to overfitting the target pseudo labels and producing unstable features. These observations indicate that an appropriate KD weight strikes the right balance by providing effective regularization while preserving the model’s capacity to adapt, thus yielding the best performance.

V. CONCLUSION AND FUTURE WORK

A. Conclusion

In this paper, we propose OMUDA, a unified masking-based framework to mitigate performance degradation in semantic segmentation under domain shift. OMUDA integrates context-aware masking for intelligent data mixing, feature distillation to promote domain-invariant representations, and category-specific masking to stabilize pseudo-label supervision and enhance feature compactness. By jointly leveraging these complementary mechanisms, OMUDA effectively strengthens cross-domain knowledge transfer. Notably, OMUDA is implemented purely as a training strategy and introduces no

additional computational overhead at inference. We believe OMUDA provides useful insights for future research in unsupervised domain adaptation and the design of more robust semantic segmentation models.

B. Limitations and Future Work

Our framework requires defining foreground–background class groups and tuning several hyperparameters, though these requirements are common in UDA research. We have provided detailed analyses to help guide these choices. Future directions include developing adaptive masking strategies that dynamically respond to domain shift severity, incorporating self-supervised objectives to further enhance representation robustness, and extending the approach to multi-source domain adaptation settings.

REFERENCES

- [1] X. Guo, W. Zhou, and T. Liu, “Contrastive learning-based knowledge distillation for rgb-thermal urban scene semantic segmentation,” *Knowledge-Based Systems*, vol. 292, p. 111588, 2024.
- [2] A. Yu, K. Gao, X. You, Y. Zhong, Y. Su, B. Liu, and C. Qiu, “Rethinking semantic segmentation with multi-grained logical prototype,” *IEEE Transactions on Image Processing*, 2025.
- [3] X. Zhao, C. Wen, X. Zhu, Y. Wang, H. Bai, and W. Dou, “Triplemixer: A triple-domain mixing model for point cloud denoising under adverse weather,” *IEEE Transactions on Image Processing*, vol. 34, pp. 7712–7727, 2025.
- [4] X. Zhao, X. Chen, X. Zhu, X. Xie, H. Bai, C. Wen, R. Zhou, and Q. Sun, “An iterative task-driven framework for resilient lidar place recognition in adverse weather,” *arXiv preprint arXiv:2504.14806*, 2025.
- [5] W. Kuang, X. Zhao, Y. Shen, C. Wen, H. Lu, Z. Zhou, and X. Chen, “Reslpr: A lidar data restoration network and benchmark for robust place recognition against weather corruptions,” *arXiv preprint arXiv:2503.12350*, 2025.
- [6] L. Yang, X. Zhao, Q. Sun, K. Wang, A. Chen, and P. Kang, “Splatpose: Geometry-aware 6-dof pose estimation from single rgb image via 3d gaussian splatting,” *arXiv preprint arXiv:2503.05174*, 2025.
- [7] A. Vijai, S. Padmavathi, and D. Venkataraman, “Artificial intelligence based semantic segmentation on aerial images with variational mode decomposition,” *Engineering Applications of Artificial Intelligence*, vol. 156, p. 111140, 2025.
- [8] W. Zhou, Y. Xiao, F. Qiang, X. Dong, C. Xu, and L. Yu, “Aeseg: Affinity-enhanced segmenter using feature class mapping knowledge distillation for efficient rgb-d semantic segmentation of indoor scenes,” *Neural Networks*, vol. 188, p. 107438, 2025.
- [9] W.-J. Ahn, G.-Y. Yang, H.-D. Choi, and M.-T. Lim, “Style blind domain generalized semantic segmentation via covariance alignment and semantic consistency contrastive learning,” in *Proceedings of the IEEE/CVF conference on computer vision and pattern recognition*, 2024, pp. 3616–3626.
- [10] T. Loiseau, T.-H. Vu, M. Chen, P. Pérez, and M. Cord, “Reliability in semantic segmentation: Can we use synthetic data?” in *European Conference on Computer Vision*. Springer, 2024, pp. 442–459.
- [11] H. Qian, Y. Chen, S. Lou, F. Shahbaz Khan, X. Jin, and D.-P. Fan, “Maskfactory: Towards high-quality synthetic data generation for dichotomous image segmentation,” *Advances in Neural Information Processing Systems*, vol. 37, pp. 66 455–66 478, 2024.
- [12] H. Tang, S. Yu, J. Pang, and B. Zhang, “A training-free synthetic data selection method for semantic segmentation,” in *Proceedings of the AAAI Conference on Artificial Intelligence*, vol. 39, no. 7, 2025, pp. 7229–7237.
- [13] J. Li, Z. Yu, Z. Du, L. Zhu, and H. T. Shen, “A comprehensive survey on source-free domain adaptation,” *IEEE Transactions on Pattern Analysis and Machine Intelligence*, 2024.
- [14] P. Oza, V. A. Sindagi, V. V. Sharmini, and V. M. Patel, “Unsupervised domain adaptation of object detectors: A survey,” *IEEE Transactions on Pattern Analysis and Machine Intelligence*, 2023.
- [15] L. Hoyer, D. Dai, H. Wang, and L. Van Gool, “Mic: Masked image consistency for context-enhanced domain adaptation,” in *Proceedings of the IEEE/CVF conference on computer vision and pattern recognition*, 2023, pp. 11 721–11 732.
- [16] Z. Du, X. Li, F. Li, K. Lu, L. Zhu, and J. Li, “Domain-agnostic mutual prompting for unsupervised domain adaptation,” in *Proceedings of the IEEE/CVF Conference on Computer Vision and Pattern Recognition*, 2024, pp. 23 375–23 384.
- [17] W. Yan, Y. Qian, H. Zhuang, C. Wang, and M. Yang, “Sam4udass: When sam meets unsupervised domain adaptive semantic segmentation in intelligent vehicles,” *IEEE Transactions on Intelligent Vehicles*, vol. 9, no. 2, pp. 3396–3408, 2023.
- [18] L. Yang, L. Hoyer, M. Weber, T. Fischer, D. Dai, L. Leal-Taixé, M. Pollefeys, D. Cremers, and L. Van Gool, “Micdrop: masking image and depth features via complementary dropout for domain-adaptive semantic segmentation,” in *European Conference on Computer Vision*. Springer, 2024, pp. 329–346.
- [19] Y. Du, Y. Shen, H. Wang, J. Fei, W. Li, L. Wu, R. Zhao, Z. Fu, and Q. Liu, “Learning from future: A novel self-training framework for semantic segmentation,” *Advances in Neural Information Processing Systems*, vol. 35, pp. 4749–4761, 2022.
- [20] Q. Zhou, Z. Feng, Q. Gu, J. Pang, G. Cheng, X. Lu, J. Shi, and L. Ma, “Context-aware mixup for domain adaptive semantic segmentation,” *IEEE Transactions on Circuits and Systems for Video Technology*, vol. 33, no. 2, pp. 804–817, 2022.
- [21] L. Yang, L. Hoyer, M. Weber, T. Fischer, D. Dai, L. Leal-Taixé, M. Pollefeys, D. Cremers, and L. Van Gool, “Micdrop: masking image and depth features via complementary dropout for domain-adaptive semantic segmentation,” in *European Conference on Computer Vision*. Springer, 2024, pp. 329–346.
- [22] X. Li, H. Ding, H. Yuan, W. Zhang, J. Pang, G. Cheng, K. Chen, Z. Liu, and C. C. Loy, “Transformer-based visual segmentation: A survey,” *IEEE transactions on pattern analysis and machine intelligence*, 2024.
- [23] C. Zhu and L. Chen, “A survey on open-vocabulary detection and segmentation: Past, present, and future,” *IEEE Transactions on Pattern Analysis and Machine Intelligence*, vol. 46, no. 12, pp. 8954–8975, 2024.
- [24] L. Ran, Y. Li, G. Liang, and Y. Zhang, “Pseudo labeling methods for semi-supervised semantic segmentation: A review and future perspectives,” *IEEE Transactions on Circuits and Systems for Video Technology*, 2024.
- [25] H. Hu, J. Cui, and L. Wang, “Region-aware contrastive learning for semantic segmentation,” in *Proceedings of the IEEE/CVF International Conference on Computer Vision*, 2021, pp. 16 291–16 301.
- [26] W. Wang, T. Zhou, F. Yu, J. Dai, E. Konukoglu, and L. Van Gool, “Exploring cross-image pixel contrast for semantic segmentation,” in *Proceedings of the IEEE/CVF international conference on computer vision*, 2021, pp. 7303–7313.
- [27] J. Peng, Y. Liu, S. Tang, Y. Hao, L. Chu, G. Chen, Z. Wu, Z. Chen, Z. Yu, Y. Du *et al.*, “Pp-liteseg: A superior real-time semantic segmentation model,” *arXiv preprint arXiv:2204.02681*, 2022.
- [28] C. Sung, W. Kim, J. An, W. Lee, H. Lim, and H. Myung, “Contextrast: Contextual contrastive learning for semantic segmentation,” in *Proceedings of the IEEE/CVF conference on computer vision and pattern recognition*, 2024, pp. 3732–3742.
- [29] M. Silva, A. Seoane, O. A. Mures, A. M. López, and J. A. Iglesias-Guitian, “Exploring the effects of synthetic data generation: a case study on autonomous driving for semantic segmentation,” *The visual computer*, pp. 1–19, 2025.
- [30] Y. Fang, P.-T. Yap, W. Lin, H. Zhu, and M. Liu, “Source-free unsupervised domain adaptation: A survey,” *Neural Networks*, p. 106230, 2024.
- [31] S. Hu, F. Bonardi, S. Bouchafa, and D. Sidibé, “Multi-modal unsupervised domain adaptation for semantic image segmentation,” *Pattern Recognition*, vol. 137, p. 109299, 2023.
- [32] M. Schwonberg, J. Niemeijer, J.-A. Termöhlen, N. M. Schmidt, H. Gottschalk, T. Fingscheidt *et al.*, “Survey on unsupervised domain adaptation for semantic segmentation for visual perception in automated driving,” *IEEE Access*, vol. 11, pp. 54 296–54 336, 2023.
- [33] Q. Tian, J. Zhou, and Y. Chu, “Joint bi-adversarial learning for unsupervised domain adaptation,” *Knowledge-Based Systems*, vol. 248, p. 108903, 2022.
- [34] Y. Yang, T. Zhang, G. Li, T. Kim, and G. Wang, “An unsupervised domain adaptation model based on dual-module adversarial training,” *Neurocomputing*, vol. 475, pp. 102–111, 2022.
- [35] T.-H. Vu, H. Jain, M. Bucher, M. Cord, and P. Pérez, “Advent: Adversarial entropy minimization for domain adaptation in semantic segmentation,” in *Proceedings of the IEEE/CVF conference on computer vision and pattern recognition*, 2019, pp. 2517–2526.
- [36] M. Wang, W. Wang, B. Li, X. Zhang, L. Lan, H. Tan, T. Liang, W. Yu, and Z. Luo, “Interbn: Channel fusion for adversarial unsupervised

- domain adaptation,” in *Proceedings of the 29th ACM international conference on multimedia*, 2021, pp. 3691–3700.
- [37] Y. Luo, L. Zheng, T. Guan, J. Yu, and Y. Yang, “Taking a closer look at domain shift: Category-level adversaries for semantics consistent domain adaptation,” in *Proceedings of the IEEE/CVF conference on computer vision and pattern recognition*, 2019, pp. 2507–2516.
- [38] Y. Luo, P. Liu, L. Zheng, T. Guan, J. Yu, and Y. Yang, “Category-level adversarial adaptation for semantic segmentation using purified features,” *IEEE Transactions on Pattern Analysis and Machine Intelligence*, vol. 44, no. 8, pp. 3940–3956, 2021.
- [39] Z. Zheng and Y. Yang, “Adaptive boosting for domain adaptation: Toward robust predictions in scene segmentation,” *IEEE Transactions on Image Processing*, vol. 31, pp. 5371–5382, 2022.
- [40] M. Chen, Z. Zheng, Y. Yang, and T.-S. Chua, “Pipa: Pixel-and patch-wise self-supervised learning for domain adaptive semantic segmentation,” in *Proceedings of the 31st ACM International Conference on Multimedia*, 2023, pp. 1905–1914.
- [41] X. Li, Y. Qiu, J. Liao, F. Meng, and P. Ren, “Unsupervised domain adaptation semantic segmentation of remote sensing images with mask enhancement and balanced sampling,” *IEEE Transactions on Geoscience and Remote Sensing*, 2025.
- [42] X. Zhao, N. C. Mithun, A. Rajvanshi, H.-P. Chiu, and S. Samarasekera, “Unsupervised domain adaptation for semantic segmentation with pseudo label self-refinement,” in *Proceedings of the IEEE/CVF Winter Conference on Applications of Computer Vision*, 2024, pp. 2399–2409.
- [43] X. Wu, Z. Wu, H. Guo, L. Ju, and S. Wang, “Dannet: A one-stage domain adaptation network for unsupervised nighttime semantic segmentation,” in *Proceedings of the IEEE/CVF Conference on Computer Vision and Pattern Recognition*, 2021, pp. 15769–15778.
- [44] Y. Zou, Z. Yu, B. Kumar, and J. Wang, “Unsupervised domain adaptation for semantic segmentation via class-balanced self-training,” in *Proceedings of the European conference on computer vision (ECCV)*, 2018, pp. 289–305.
- [45] Y. Zou, Z. Yu, X. Liu, B. Kumar, and J. Wang, “Confidence regularized self-training,” in *Proceedings of the IEEE/CVF international conference on computer vision*, 2019, pp. 5982–5991.
- [46] P. Zhang, B. Zhang, T. Zhang, D. Chen, Y. Wang, and F. Wen, “Prototypical pseudo label denoising and target structure learning for domain adaptive semantic segmentation,” in *Proceedings of the IEEE/CVF conference on computer vision and pattern recognition*, 2021, pp. 12414–12424.
- [47] Y. Zhao, Z. Zhong, Z. Luo, G. H. Lee, and N. Sebe, “Source-free open compound domain adaptation in semantic segmentation,” *IEEE Transactions on Circuits and Systems for Video Technology*, vol. 32, no. 10, pp. 7019–7032, 2022.
- [48] N. Araslanov and S. Roth, “Self-supervised augmentation consistency for adapting semantic segmentation,” in *Proceedings of the IEEE/CVF Conference on Computer Vision and Pattern Recognition*, 2021, pp. 15384–15394.
- [49] K. Wang, D. Kim, R. Feris, K. Saenko, and M. Betke, “Exploring consistency in cross-domain transformer for domain adaptive semantic segmentation,” *arXiv preprint arXiv:2211.14703*, 2022.
- [50] G. Lee, C. Eom, W. Lee, H. Park, and B. Ham, “Bi-directional contrastive learning for domain adaptive semantic segmentation,” in *European Conference on Computer Vision*. Springer, 2022, pp. 38–55.
- [51] W. Liu, D. Ferstl, S. Schuster, L. Zebadin, P. Fua, and C. Leistner, “Domain adaptation for semantic segmentation via patch-wise contrastive learning,” *arXiv preprint arXiv:2104.11056*, 2021.
- [52] W. Tranheden, V. Olsson, J. Pinto, and L. Svensson, “Dacs: Domain adaptation via cross-domain mixed sampling,” in *Proceedings of the IEEE/CVF Winter Conference on Applications of Computer Vision*, 2021, pp. 1379–1389.
- [53] Z. Zhang, G. Wu, J. Zhang, X. Zhu, D. Tao, and T. Chai, “Unified domain adaptive semantic segmentation,” *IEEE transactions on pattern analysis and machine intelligence*, 2025.
- [54] Y. Cheng, F. Wei, J. Bao, D. Chen, F. Wen, and W. Zhang, “Dual path learning for domain adaptation of semantic segmentation,” in *Proceedings of the IEEE/CVF international conference on computer vision*, 2021, pp. 9082–9091.
- [55] X. Lu, L. Li, L. Jiao, X. Liu, F. Liu, W. Ma, and S. Yang, “Uncertainty-aware semi-supervised learning segmentation for remote sensing images,” *IEEE Transactions on Multimedia*, 2025.
- [56] H. Yin, P. Wang, B. Liu, and J. Yan, “An uncertainty-aware domain adaptive semantic segmentation framework,” *Autonomous Intelligent Systems*, vol. 4, no. 1, p. 15, 2024.
- [57] Z. Zheng and Y. Yang, “Rectifying pseudo label learning via uncertainty estimation for domain adaptive semantic segmentation,” *International Journal of Computer Vision*, vol. 129, no. 4, pp. 1106–1120, 2021.
- [58] S. R. Richter, V. Vineet, S. Roth, and V. Koltun, “Playing for data: Ground truth from computer games,” in *Computer Vision—ECCV 2016: 14th European Conference, Amsterdam, The Netherlands, October 11–14, 2016, Proceedings, Part II 14*. Springer, 2016, pp. 102–118.
- [59] G. Ros, L. Sellart, J. Materzynska, D. Vazquez, and A. M. Lopez, “The synthia dataset: A large collection of synthetic images for semantic segmentation of urban scenes,” in *Proceedings of the IEEE conference on computer vision and pattern recognition*, 2016, pp. 3234–3243.
- [60] M. Cordts, M. Omran, S. Ramos, T. Rehfeld, M. Enzweiler, R. Benenson, U. Franke, S. Roth, and B. Schiele, “The cityscapes dataset for semantic urban scene understanding,” in *Proceedings of the IEEE conference on computer vision and pattern recognition*, 2016, pp. 3213–3223.
- [61] L. Hoyer, D. Dai, and L. Van Gool, “Daformer: Improving network architectures and training strategies for domain-adaptive semantic segmentation,” in *Proceedings of the IEEE/CVF Conference on Computer Vision and Pattern Recognition*, 2022, pp. 9924–9935.
- [62] E. Xie, W. Wang, Z. Yu, A. Anandkumar, J. M. Alvarez, and P. Luo, “Segformer: Simple and efficient design for semantic segmentation with transformers,” *Advances in Neural Information Processing Systems*, vol. 34, pp. 12077–12090, 2021.
- [63] J. Deng, W. Dong, R. Socher, L.-J. Li, K. Li, and L. Fei-Fei, “Imagenet: A large-scale hierarchical image database,” in *2009 IEEE conference on computer vision and pattern recognition*. Ieee, 2009, pp. 248–255.
- [64] I. Loshchilov and F. Hutter, “Decoupled weight decay regularization,” *arXiv preprint arXiv:1711.05101*, 2017.
- [65] P. Goyal, P. Dollár, R. Girshick, P. Noordhuis, L. Wesolowski, A. Kyrola, A. Tulloch, Y. Jia, and K. He, “Accurate, large minibatch sgd: Training imagenet in 1 hour,” *arXiv preprint arXiv:1706.02677*, 2017.
- [66] H. Wang, T. Shen, W. Zhang, L.-Y. Duan, and T. Mei, “Classes matter: A fine-grained adversarial approach to cross-domain semantic segmentation,” in *European conference on computer vision*. Springer, 2020, pp. 642–659.
- [67] Y. Yang and S. Soatto, “Fda: Fourier domain adaptation for semantic segmentation,” in *Proceedings of the IEEE/CVF conference on computer vision and pattern recognition*, 2020, pp. 4085–4095.
- [68] Q. Wang, D. Dai, L. Hoyer, L. Van Gool, and O. Fink, “Domain adaptive semantic segmentation with self-supervised depth estimation,” in *Proceedings of the IEEE/CVF International Conference on Computer Vision*, 2021, pp. 8515–8525.
- [69] T. Li, S. Roy, H. Zhou, H. Lu, and S. Lathuilière, “Contrast, stylize and adapt: Unsupervised contrastive learning framework for domain adaptive semantic segmentation,” in *Proceedings of the IEEE/CVF conference on computer vision and pattern recognition*, 2023, pp. 4869–4879.
- [70] Y. Wang, J. Liang, J. Xiao, S. Mei, Y. Yang, and Z. Zhang, “Informative data mining for one-shot cross-domain semantic segmentation,” in *Proceedings of the IEEE/CVF International Conference on Computer Vision*, 2023, pp. 1064–1074.
- [71] G. Li, G. Kang, W. Liu, Y. Wei, and Y. Yang, “Content-consistent matching for domain adaptive semantic segmentation,” in *European conference on computer vision*. Springer, 2020, pp. 440–456.
- [72] C. Hümmer, M. Schwonberg, L. Zhou, H. Cao, A. Knoll, and H. Gottschalk, “Vltseg: Simple transfer of clip-based vision-language representations for domain generalized semantic segmentation,” *arXiv preprint arXiv:2312.02021*, 2023.
- [73] B. Pak, B. Woo, S. Kim, D.-h. Kim, and H. Kim, “Textual query-driven mask transformer for domain generalized segmentation,” in *European Conference on Computer Vision*. Springer, 2024, pp. 37–54.
- [74] S. Jeon, K. Hong, and H. Byun, “Exploiting domain properties in language-driven domain generalization for semantic segmentation,” in *Proceedings of the IEEE/CVF International Conference on Computer Vision*, 2025, pp. 20791–20801.
- [75] L. Van der Maaten and G. Hinton, “Visualizing data using t-sne,” *Journal of machine learning research*, vol. 9, no. 11, 2008.
- [76] Z. Xie, Z. Zhang, Y. Cao, Y. Lin, J. Bao, Z. Yao, Q. Dai, and H. Hu, “Simmim: A simple framework for masked image modeling,” in *Proceedings of the IEEE/CVF conference on computer vision and pattern recognition*, 2022, pp. 9653–9663.
- [77] P. Chen, S. Liu, H. Zhao, and J. Jia, “Gridmask data augmentation,” *arXiv preprint arXiv:2001.04086*, 2020.